UNIVERSITY *of York*

This is a repository copy of *The Structure of the Cysteine-Rich Domain of Plasmodium falciparum P113 Identifies the Location of the RH5 Binding Site.*.

White Rose Research Online URL for this paper:
https://eprints.whiterose.ac.uk/id/eprint/166894/

Version: Published Version

Article:

White Rose
university consortium
Universities of Leeds, Sheffield & York

eprints@whiterose.ac.uk
https://eprints.whiterose.ac.uk/

The Structure of the Cysteine-Rich Domain of *Plasmodium falciparum* P113 Identifies the Location of the RH5 Binding Site

Ivan Campeotto,[a,b] Francis Galaway,[c] Shahid Mehmood,[d] Lea K. Barfod,[e] Doris Quinkert,[e] Vinayaka Kotraiah,[f] Timothy W. Phares,[f] Katherine E. Wright,[a] Ambrosius P. Snijders,[d] Simon J. Draper,[e] Matthew K. Higgins,[a] Gavin J. Wright[c]

aDepartment of Biochemistry, University of Oxford, Oxford, United Kingdom
bDepartment of Biochemistry, Nottingham Trent University, Nottingham, United Kingdom
cCell Surface Signalling Laboratory, Wellcome Trust Sanger Institute, Cambridge, United Kingdom
dProtein Analysis and Proteomics Platform, The Francis Crick Institute, London, United Kingdom
eThe Jenner Institute, University of Oxford, Oxford, United Kingdom
fLeidos Life Sciences, Leidos Inc., Frederick, Maryland, USA

Ivan Campeotto and Francis Galaway contributed equally. Author order was determined by mutual agreement.

ABSTRACT *Plasmodium falciparum* RH5 is a secreted parasite ligand that is essential for erythrocyte invasion through direct interaction with the host erythrocyte receptor basigin. RH5 forms a tripartite complex with two other secreted parasite proteins, CyRPA and RIPR, and is tethered to the surface of the parasite through membrane-anchored P113. Antibodies against RH5, CyRPA, and RIPR can inhibit parasite invasion, suggesting that vaccines containing these three components have the potential to prevent blood-stage malaria. To further explore the role of the P113-RH5 interaction, we selected monoclonal antibodies against P113 that were either inhibitory or noninhibitory for RH5 binding. Using a Fab fragment as a crystallization chaperone, we determined the crystal structure of the RH5 binding region of P113 and showed that it is composed of two domains with structural similarities to rhamnose-binding lectins. We identified the RH5 binding site on P113 by using a combination of hydrogen-deuterium exchange mass spectrometry and site-directed mutagenesis. We found that a monoclonal antibody to P113 that bound to this interface and inhibited the RH5-P113 interaction did not inhibit parasite blood-stage growth. These findings provide further structural information on the protein interactions of RH5 and will be helpful in guiding the development of blood-stage malaria vaccines that target RH5.

IMPORTANCE Malaria is a deadly infectious disease primarily caused by the parasite *Plasmodium falciparum*. It remains a major global health problem, and there is no highly effective vaccine. A parasite protein called RH5 is centrally involved in the invasion of host red blood cells, making it—and the other parasite proteins it interacts with—promising vaccine targets. We recently identified a protein called P113 that binds RH5, suggesting that it anchors RH5 to the parasite surface. In this paper, we use structural biology to locate and characterize the RH5 binding region on P113. These findings will be important to guide the development of new antimalarial vaccines to ultimately prevent this disease, which affects some of the poorest people on the planet.

Malaria is a devastating infectious disease caused by parasites from the genus *Plasmodium*, and in 2018, it was responsible for an estimated 228 million clinical cases (1). Over 99% of malaria cases are caused by *Plasmodium falciparum*, a parasite that is endemic in many tropical regions and is responsible for over 400,000 deaths each year (1). While several licensed drugs kill *Plasmodium* parasites, the requirement to treat each new infection, and the emergence of drug-resistant parasites, threatens current control methods (2). A vaccine that elicits high levels of long-lasting protection will be a valuable tool in the battle against malaria.

The symptoms of malaria occur when the parasite replicates within human blood. This is initiated when the merozoite form of *Plasmodium* recognizes and invades a host erythrocyte. Invasion requires molecular interactions between parasite ligands, which are released in an ordered schedule from intracellular organelles, and receptor proteins displayed on host erythrocyte surfaces (3, 4). As erythrocyte invasion is an essential stage of the parasite life cycle, and the merozoite is directly exposed to host antibodies, invasion has long been considered a suitable target for vaccine-elicited antibodies. An important advance in targeting the blood stage was the discovery that the parasite protein reticulocyte-binding protein homologue 5 (RH5), makes an interaction with erythrocyte basigin which is essential and universally required by all strains of parasite for invasion (5). This interaction has been structurally characterized (6), and studies have shown that anti-RH5 antibodies can prevent erythrocyte invasion by multiple *Plasmodium falciparum* strains (7–9). Vaccination of nonhuman primates with RH5 protected them from challenge with a heterologous parasite strain (10), and anti-RH5 monoclonal antibodies (MAbs) can passively protect nonhuman primates (11). While human clinical trials of RH5 are under way (12), the analysis of antibodies, elicited through human vaccination, has been instructive in revealing the epitopes of protective and potentiating antibodies which should be induced by future focused vaccines (7).

RH5 does not act alone on the surface of the merozoite but forms a tripartite complex with two other secreted parasite proteins: cysteine-rich protective antigen (CyRPA) (13–15) and RH5-interacting protein (RIPR) (16). Prior to invasion, these proteins are spatially segregated: RH5 is sequestered within the rhoptry (17) and both CyRPA and RIPR are localized to the micronemes (15). The proteins ultimately colocalize, most likely at the point of invasion, and the complex has been studied using recombinant proteins in binary protein interaction assays (18) and its architecture determined to 7-Å resolution (19). Recently, a fourth interacting partner of RH5 was identified as an abundant glycosylphosphatidylinositol (GPI)-anchored merozoite surface protein called P113. P113 has been localized to the merozoite surface (18, 20), as well as to the parasitophorous vacuole (21, 22), and was shown to tether the RH5:CyRPA:RIPR complex to the merozoite surface (18). The interaction is conserved across the *Laverania* subgenus (23), and the core of the interaction was mapped to the N-terminal region of P113 (residues 1 to 197) and a 19-residue peptide from the flexible and disordered N terminus of RH5 (residues 9 to 27) which does not interact with RIPR or CyRPA. Polyclonal antibodies raised against the RH5 N terminus (residues 1 to 116) inhibited the interaction with P113 and also inhibited parasite growth *in vitro* (18). It was not known, however, whether antibodies that target P113 and prevent it from binding to RH5 would also prevent erythrocyte invasion. We therefore raised monoclonal antibodies against P113 which are inhibitory and noninhibitory for RH5 binding and have used these to understand the molecular basis for the P113:RH5 interaction and to assess the importance of this interaction as a vaccine target.

RESULTS

Selection and characterization of monoclonal antibodies that bind the N-terminal region of P113. To functionally and structurally investigate the interaction between P113 and RH5, we first selected mouse monoclonal antibodies to *P. falciparum* P113. Antibodies were first tested by enzyme-linked immunosorbent assay (ELISA) to identify those which bind to the N-terminal cysteine-rich region of P113 which contains the RH5 binding site (18) and then for their ability to block binding to RH5. For this
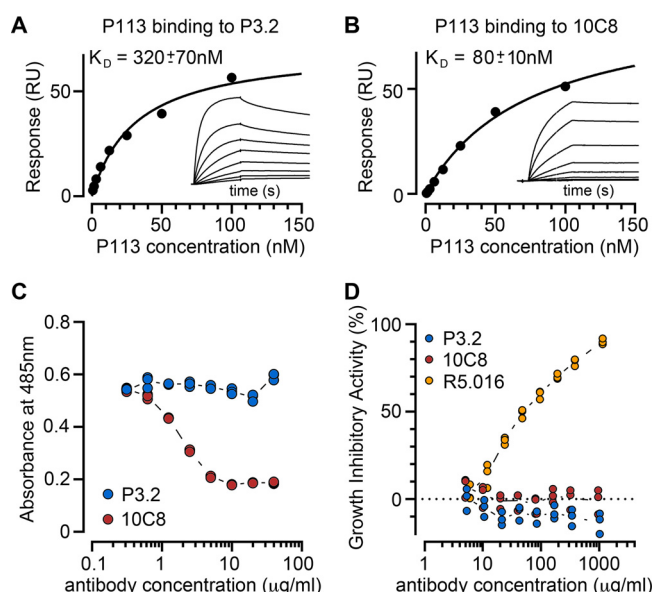
FIG 1 Monoclonal antibodies against P113 that block and do not block RH5 binding do not inhibit parasite growth *in vitro*. (A and B) Binding kinetics of the anti-P113 monoclonal antibodies P3.2 (A) and 10C8 (B) to the P113 N-terminal fragment were assessed by surface plasmon resonance. Each monoclonal antibody was immobilized on the sensor surface, and the binding parameters of a dilution series of the purified P113 N-terminal fragment were quantified. The response once equilibrium had been reached was plotted, and equilibrium dissociation constants (K_Ds) were calculated by nonlinear curve fitting to the data. Raw sensorgrams are shown in the inset. (C) Anti-P113 MAb 10C8 inhibits P113 from binding to RH5 in an AVEXIS assay, but P3.2 does not. The indicated concentrations of protein G-purified monoclonal antibodies were incubated with the biotinylated P113 N-terminal fragment immobilized in wells of a streptavidin-coated microtiter plate before presenting the RH5 beta-lactamase-tagged prey protein; prey binding was quantified by the hydrolysis of the colorimetric beta-lactamase substrate at 485 nm. At the antibody concentrations tested, P3.2 did not inhibit the P113-RH5 interaction while 10C8 blocked the interaction. Triplicate data points for each antibody concentration from representative experiments are shown. (D) Neither RH5 blocking (10C8) nor nonblocking (P3.2) anti-P113 monoclonal antibodies inhibit invasion of erythrocytes in a *P. falciparum* blood-stage growth inhibition assay. Synchronized mid-stage trophozoites were added to erythrocytes in the presence of dilution series of 10C8 and P3.2 antibodies. The anti-RH5 MAb R5.016 is included as a positive control. Triplicate data points for each antibody concentration are shown.

study, we selected two anti-P113 monoclonal antibodies: one that could block the interaction with RH5 (10C8) and one that could not (P3.2) (Fig. 1). We used surface plasmon resonance (SPR) to quantify the binding of both antibodies to the soluble N-terminal region of P113. Both bound to P113 with nanomolar affinity (10C8, K_D [equilibrium dissociation constant] = 80 nM; P3.2, K_D = 320 nM) (Fig. 1A and B). Using the AVEXIS binding assay (24), we assessed their ability to prevent P113 from binding to RH5. We found that 10C8 blocked the interaction with RH5 while P3.2 did not (Fig. 1C). Because antibodies to RH5 prevent the invasion of erythrocytes by *P. falciparum*, we next asked if there was a correlation between the ability of the anti-P113 antibodies to block the RH5 interaction and the ability to prevent invasion. By adding serial dilutions of both monoclonal antibodies to a parasite growth inhibition activity (GIA) assay, we found that neither anti-P113 monoclonal antibody was able to inhibit parasite growth in blood culture, even at concentrations that far exceeded the concentrations needed to inhibit the interaction *in vitro* and at which a monoclonal antibody targeting RH5 (R5.016) (7) showed >90% growth inhibition (Fig. 1D).

Crystal structure of the N-terminal domains of P113. To better understand the function of the N-terminal region of P113, we determined its crystal structure. A protein containing residues 1 to 197 was expressed in HEK293 cells and purified for crystallization. While this did not crystallize alone, we were able to use a Fab fragment of the noninhibitory P3.2 antibody as a crystallization chaperone. A complex of P113 residues 1 to 197 bound to the P3.2 Fab fragment formed crystals that diffracted to 1.95-Å
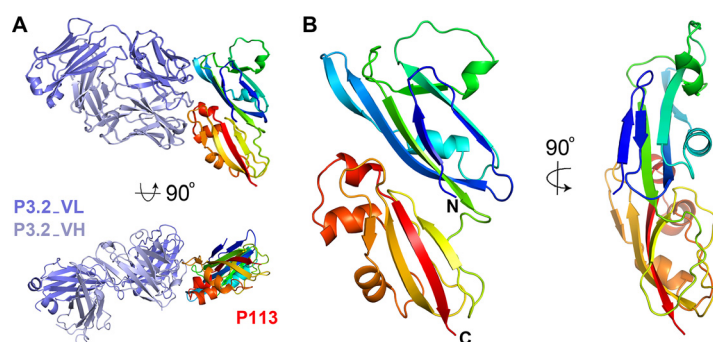
FIG 2 The structure of the N-terminal region of P113. (A) The structure of residues 1 to 197 of P113 bound to the Fab fragment of monoclonal antibody P3.2. P113 is shown in rainbow representation, from blue at the N terminus through to red at the C terminus. The P3.2 Fab fragment is shown in dark and light blue for the light and heavy chains, respectively. (B) Two views of P113$_{1-197}$, colored as in panel A.

resolution. The structure was determined by molecular replacement, using the structure of the Fab fragment of antibody 9AD4 (6) as a search model, followed by iterative cycles of building and refinement, starting with a polyalanine model of P113. The noninhibitory antibody, P3.2, bound to an epitope on the narrower side of P113 (Fig. 2). Both heavy and light chains are involved in binding, and the epitope has a surface area of ~850 Å^2 (638 Å^2 from V$_H$ and 212 Å^2 from V$_L$), with the interaction involving 15 hydrogen bonds, together with surface charge complementarity.

The structure of the N-terminal region of P113 reveals two closely interacting domains. Both are formed from a four-stranded antiparallel β-sheet which packs against an α-helix (Fig. 2 and 3). Long loops at one end adopt different structures containing one or two short α-helices with the domains showing an overall root mean square deviation of 3.2 Å compared with each other. In architecture, both domains

P113_domain 1 : **P113_domain 2** : latrophilin 1_lectin : **CSL3_lectin**
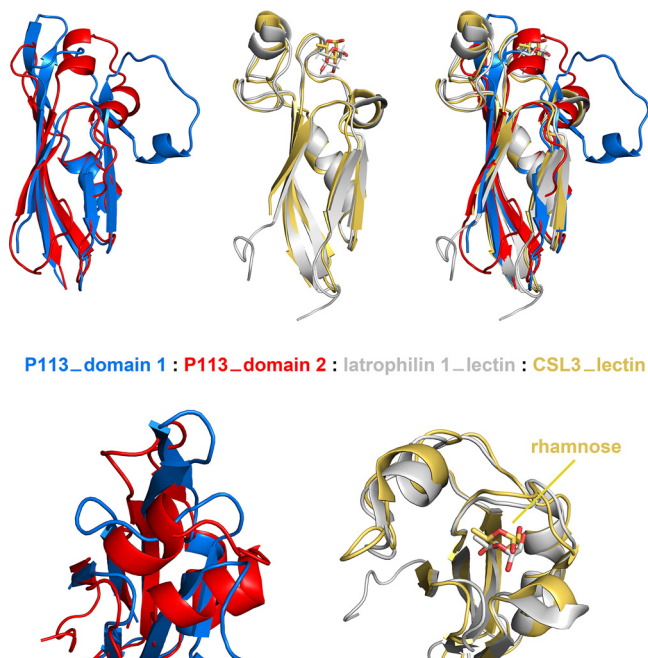
FIG 3 The two domains of P113 resemble rhamnose-binding lectins but lack residues required for rhamnose binding. A comparison of the structures of domains 1 (blue) and 2 (red) of P113 with rhamnose-binding lectin domains. The structures of the lectin domains of latrophilin 1 (PDB: 2JXA, gray) and CSL3 (PDB: 2ZX2, yellow) are shown in complex with the monosaccharide rhamnose. The lower panel shows a closeup view of the rhamnose-binding pockets of the lectins (right) and the equivalent regions of the P113 domains (left).

closely resemble the rhamnose-binding lectin domains, found in proteins such as CSL3 (25), latrophilin (26), and FLRT (27) (Fig. 3). However, structural differences in the region of the rhamnose binding site make it very unlikely that P113 is a rhamnose-binding lectin. Structures of lectin domains from CSL3 (25) and latrophilin (26), in complex with rhamnose, show that these domains share a GTY motif that orders the loop surrounding the lectin binding site (Fig. 3). The GTY motif is lacking in both domains of P113, causing this region of the domain to adopt a different architecture, which does not form a binding pocket for rhamnose. We therefore conclude that despite their architectural similarity, P113 is unlikely to act as a lectin.

Identification of the RH5 binding site on P113. We next aimed to understand the locations of the binding sites on P113 for RH5 and for the inhibitory antibody 10C8. We attempted to crystallize P113$_{1-197}$ in complex with the Fab fragment of 10C8, with RH5, or with a peptide containing residues 9 to 27 of RH5 previously shown to contain the P113 binding site (18). As these extensive attempts were unsuccessful, we next turned to hydrogen-deuterium exchange mass spectrometry (HDX-MS) to quantify the rate of deuterium exchange of peptides from P113 in the presence and absence of RH5 or 10C8.

The equilibrium binding affinity of full-length RH5 to P113 in solution is 0.3 μM (18); however, addition of RH5 at a concentration of 20 μM caused no significant change in the deuterium exchange of P113 peptides. This lack of protection is consistent with a small binding interface in which the RH5 peptide does not cover a sufficiently large surface area on P113 to alter deuterium exchange. In contrast, we observed reduced deuterium exchange in a number of P113 peptides from residues 103 to 114 (Fig. 4A), including 104 to 109 (Fig. 4B) in the presence of the blocking 10C8 antibody Fab fragment. Labeling these protected peptides on the crystal structure revealed the core of the 10C8 epitope on the surface of P113, which was located on the opposite side of the domain from the nonblocking P3.2 binding site (Fig. 4C).

As antibody 10C8 reduces RH5 binding, we hypothesized that their binding sites overlap. We therefore designed two structure-guided mutants and used the AVEXIS binding assay (24) to test their effect on binding to antibodies P3.2 and 10C8, as well as to RH5. To disrupt 10C8 binding, we selected two neighboring acidic residues on P113 (at positions 106 and 107), located in a solvent-exposed part of the epitope, and mutated both to lysine (D106K E107K). As a control, we made a second mutant with a charge switch mutation within the P3.2 binding epitope (E144R) (Fig. 4D). Both mutant proteins were expressed, and their ability to bind to P3.2 and 10C8 was determined. The E144R mutation abolished P3.2 binding, confirming the location of the P3.2 epitope (Fig. 4E), whereas the D106K E107K mutant caused a small but reproducible reduction of 10C8 binding, demonstrating that the 10C8 epitope was partially affected by this mutation (Fig. 4F). Both P113 mutants bound to at least one of the antibodies, suggesting no major disruption to P113 folding.

We then used these mutants to investigate the location of the RH5 binding site on P113 using the AVEXIS assay. We observed that RH5 binding to E144R was indistinguishable from that to wild type whereas the binding to the D106K E107K mutant was reduced almost to the level of the negative control (Fig. 4G). To confirm and quantify these findings, we measured the binding affinity of a purified monomeric RH5 protein to each mutant using surface plasmon resonance and observed an approximately 2-fold reduction in dissociation half-life (Fig. 4H). Together, these data localize the binding interface of RH5 on P113; one possible location is the groove formed at the interface of domains 1 and 2, which lies in close proximity to residues D106 and E107 (Fig. 4D).

DISCUSSION

In this study, we analyzed two monoclonal antibodies which target P113, allowing us to characterize the molecular basis for the interaction between P113 and RH5. First, we used a Fab fragment from the noninhibitory antibody, P3.2, as a crystallization chaperone to determine the structure of the RH5 binding region of P113. This revealed
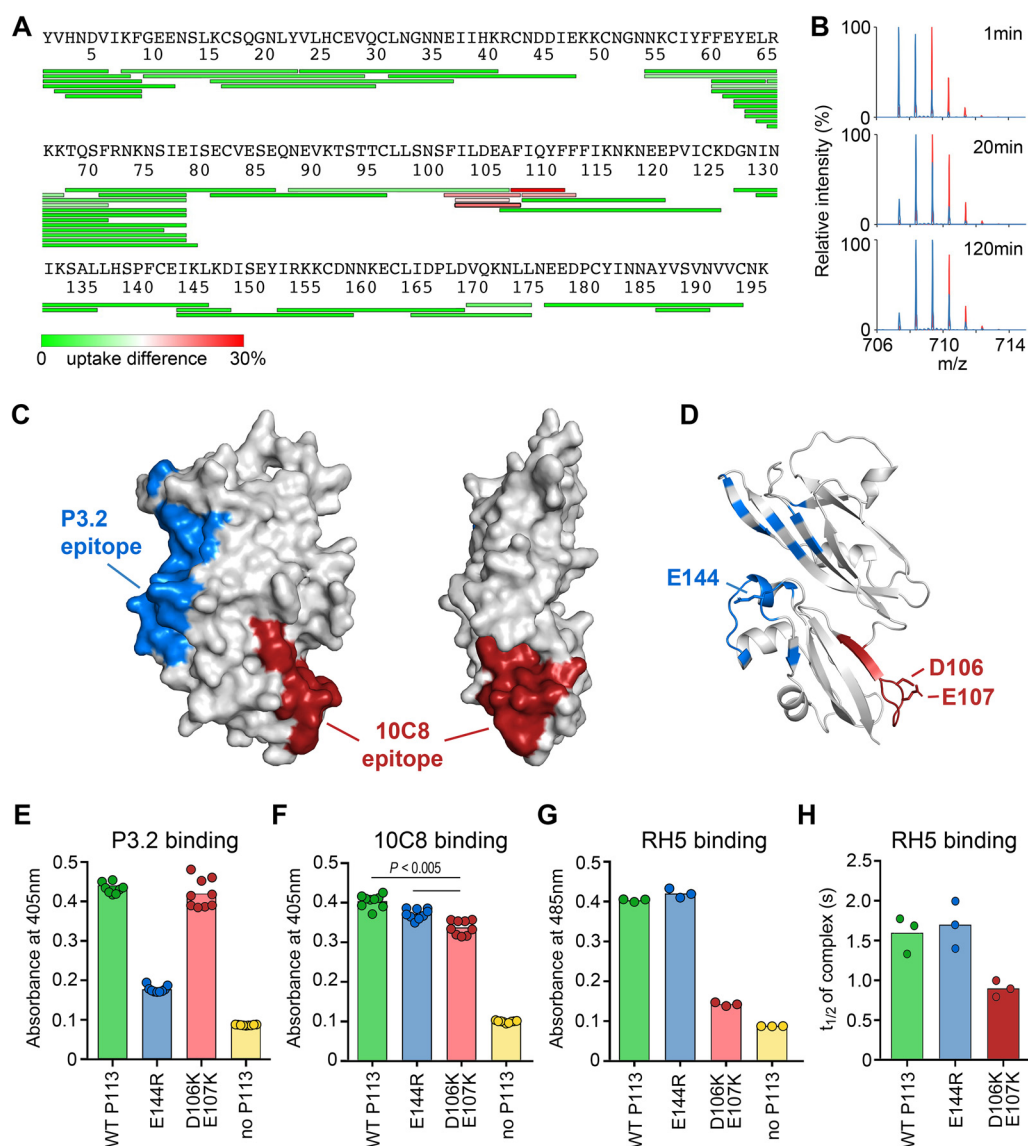
FIG 4 Localization of the RH5 binding site on P113. (A) The differences in deuterium uptake of peptides from P113 in the presence of 10C8 after 20 s of deuteration. (B) Mass spectra of P113 peptide 104 to 109, at different time periods after the start of deuteration in the absence (red) and presence (blue) of 10C8. (C) A surface representation of the P113 N-terminal domain showing the locations of the anti-P113 MAb epitopes. The epitope for P3.2, as determined from the cocrystal structure, is indicated in blue, and the core of the epitope for 10C8, as determined by HDX-MS mapping, is labeled in red. (D) The location of mutated residues on the structure of P113. (E and F) Mapping the epitopes of P3.2 (E) and 10C8 (F) using mutant P113 proteins by ELISA. The indicated mutant and wild-type (WT) P113 N-terminal domains were expressed as biotinylated proteins and immobilized on a streptavidin-coated plate, and the binding of P3.2 and 10C8 was quantified by ELISA. The E144R mutant bound 10C8 but not P3.2; the D106K;E107K mutant bound both P3.2 and 10C8, although binding to 10C8 was reduced (unpaired two-tailed t test, $P < 0.005$). (G) Location of the RH5 binding site on P113. Biotinylated wild-type and mutant P113 proteins were immobilized on a streptavidin-coated plate and probed for interactions with a pentameric beta-lactamase-tagged RH5 prey protein using the AVEXIS assay. RH5 bound the E144R mutant indistinguishably from wild type, but binding to the D106K E107K mutant was much reduced. (H) Reduction in binding half-life of RH5 to the D106K E107K mutant as determined by surface plasmon resonance. Interaction half-lives were calculated from the dissociation rate constants determined by fitting the binding data from a dilution series of purified RH5 to the P113 variants to a simple 1:1 binding model. Individual data points from representative experiments are shown; bars represent means.

that the N-terminal RH5 binding region of P113 consists of two closely packed domains, both of which have structural similarities to rhamnose-binding lectins. Despite this architectural similarity, the differences in the domain structure in the location of the rhamnose binding site make it unlikely that P113 shares their sugar-binding properties.

Despite extensive attempts, we were unable to crystallize P113$_{1-197}$ in complex with

either inhibitory antibody 10C8, the P113-binding peptide from RH5, or full-length RH5. Nevertheless, a combination of hydrogen-deuterium exchange mass spectrometry and site-directed mutagenesis allowed us to map the core of their overlapping binding sites on the opposite face of P113 from the P3.2 binding site. A groove immediately adjacent to this 10C8 epitope is a potential binding site for the N-terminal region of RH5.

It seems unlikely that the sole function of P113 is to tether RH5 to the merozoite surface because the genes encoding these two proteins do not universally cooccur in parasite genomes: genes encoding P113 orthologues are present in all sequenced *Plasmodium* species whereas RH5 is restricted to the *Laverania* subgenus. As well as being localized to the merozoite surface (18, 20, 28, 29), P113 is also associated with the membrane surrounding the parasitophorous vacuole (21, 22), where it has a role in organizing the PTEX protein export machinery (21). When more direct binding partners are determined, methods similar to those used here will allow their binding sites to be mapped onto the P113 structure.

Our studies also have consequences for the development of vaccines to prevent blood-stage malaria. RH5 and its binding partners have been identified as the most promising candidates for the development of such a vaccine (30, 31). Indeed, RH5 vaccination or passive transfer of RH5 antibodies can elicit protection against *P. falciparum* challenge in nonhuman primates (10, 11) and vaccination of human volunteers induces production of antibodies with potent growth-inhibitory activity (7, 12). As the RH5 binding partners, CyRPA and RIPR are also the targets of antibodies that are inhibitory to parasite growth; this raised the question of whether it is desirable to include P113 as part of a blood-stage malaria vaccine. Supporting this strategy were data which showed that polyclonal antibodies that target the flexible N terminus of RH5 both prevent P113 binding and inhibit parasite growth *in vitro* (18). However, our studies caution against this approach, as a monoclonal antibody which targets P113 and blocks RH5 binding was not inhibitory to invasion by *P. falciparum* into erythrocytes.

How can it be that anti-P113 antibodies which prevent the RH5:P113 interaction are not growth inhibitory? One possibility might be that this interaction is established before P113 is exposed to antibodies on the merozoite surface. Prior to invasion, the proteins of the RH5-containing complex are segregated, with RH5 localizing to the rhoptries (17), both CyRPA and RIPR localizing to the micronemes (15), and P113 being embedded in the merozoite plasma membrane (18). It is therefore not known whether these components will be accessible to antibodies before they have formed a stable complex. Indeed, epitopes for structurally characterized RH5 antibodies with growth-inhibitory activity are all found on surfaces of RH5 which remain exposed in its complex with CyRPA and RIPR (6, 7, 19, 30), and lie in the region of the basigin binding site. One possibility is that antibodies that would prevent formation of the RH5:P113 complex cannot access P113 until the complex has already formed. Whatever the reasons, the data presented in this study provide greater insight into the molecular basis for the RH5:P113 interaction but do not support the inclusion of P113 in a subunit blood-stage malaria vaccine.

MATERIALS AND METHODS

Production of protein for binding studies. The N-terminal region of the 3D7 strain *P. falciparum* P113 protein was expressed by transient transfection of HEK293 cells using the expression plasmids described in reference 23. Briefly, the P113 expression plasmids were chemically synthesized using codons optimized for expression in human cells, with potential N-linked glycosylation sites mutated, and with a C-terminal rat Cd4d3+4 tag (32). Where appropriate, monomeric "bait" proteins were enzymatically monobiotinylated by cotransfection with a plasmid encoding a secreted BirA enzyme (24, 33). To make mutations in the P113 sequence, PCR primers were designed with the intended nucleotide change and site-directed mutagenesis was performed using KOD Hot Start DNA polymerase, per the manufacturer's instructions. His-tagged proteins were purified from supernatants on HisTrap HP columns using ÄKTA pure (GE Healthcare) and resolved by gel filtration on a Superdex 200 Increase 10/300 column (GE Healthcare) (34).

Protein production for crystallization. To produce P113$_{1-197}$ for crystallization studies, the gene fragment comprising the first 591 bp of the *P113* gene sequence, previously codon optimized for expression in *Homo sapiens* (GeneArt), was subcloned into the P113-bio vector (plasmid 47729; Addgene)

using a Gibson assembly cloning kit (NEB). Primers were designed to introduce a thrombin site between the *P113* gene fragment and the coding sequence for Cd4-His$_6$ on the P113-bio vector. The resulting plasmid DNA construct was used to transfect Expi293F human cells using the Expi293F transfection kit and Expi293F expression medium (Thermo Fisher). Cells were harvested by centrifugation at $1,000 \times g$ for 30 min and resuspended in $1\times$ phosphate-buffered saline (PBS) supplemented with 30 mM imidazole. Cell lysis was performed using a cell disruptor at 10 kpsi pressure, and the cell lysate was centrifuged at $50,000 \times g$ for 30 min at 4°C. The soluble fraction was incubated for 1 h at 4°C using a Ni-NTA (nitrilotriacetic acid) resin (Qiagen). The resin was washed with 4 resin volumes (RV) of buffer A followed by elution with 3 RV of $1\times$ PBS supplemented with 0.5 M imidazole. The eluted protein was desalted against $1\times$ PBS buffer and digested with thrombin protease (GE Healthcare) in a ratio of 1 unit per μg at room temperature (RT). The reaction mixture was loaded into a gravity flow column preloaded with Ni-NTA beads to remove Cd4-His6, obtaining tagless P113$_{1-197}$.

Monoclonal antibody generation. To generate monoclonal antibody P3.2, female BALB/c mice were used (Harlan Laboratories, Oxfordshire, United Kingdom). All procedures on mice were performed in accordance with the terms of the UK Animals (Scientific Procedures) Act Project Licence and were approved by the University of Oxford Animal Welfare and Ethical Review Body. Mice were immunized intramuscularly (i.m.) with 20 μg of the entire ectodomain of P113 (18) adjuvanted in a 1:1 ratio of AddaVax (InvivoGen; catalog no. vac-adx-10) followed by two similar i.m. boosts at 2-week intervals, followed by a final intraperitoneal (i.p.) boost in PBS, 2 weeks later. Three days after the final i.p. boost, the mice were culled and spleens and blood were collected. Splenocytes were isolated by shredding the spleen through a mesh followed by washing three times in ClonaCell-HY Medium B (Stemcell Technologies). Splenocytes were fused to SP2/0 cells using the ClonaCell-HY hybridoma kit (Stemcell Technologies; catalog no. 03800). In brief, washed spleen cells and SP2/0 cells were mixed in a 5:1 ratio, pelleted, and carefully resuspended in ClonaCell-HY polyethylene glycol (PEG) solution followed by centrifugation at $133 \times g$ for 3 min. PEG solution was aspirated, and cells were resuspended initially in ClonaCell-HY Medium B and thereafter in ClonaCell-HY Medium C (Stemcell Technologies) and incubated overnight (37°C, 5% CO$_2$). On the following day, cells were pelleted (10 min at $400 \times g$), resuspended in 10 ml ClonaCell-HY Medium C and 90 ml ClonaCell-HY medium D (semisolid HAT-selection media), and plated out into 100-mm petri plates. On day 13, colonies were picked manually and transferred to HT-selection media. Culture supernatants were screened for specificity by ELISA, and positive cultures were single cell sorted using a Beckman Coulter Legacy MoFlo MLS high-speed cell sorter (BD). Monoclonal cultures were expanded in Dulbecco modified Eagle medium (DMEM) (Sigma) containing L-glutamine, penicillin-streptomycin (Pen/Strep), and ultralow fetal calf serum (FCS), and antibodies were purified from the supernatant by gravity flow protein G columns. For monoclonal antibody production, hybridoma cells were pelleted at $1,000 \times g$ and the supernatant containing antibody P3.2 was filtered with 0.22-μm filter units (Nalgene) before being loaded onto Protein G resin (Thermo Fisher) previously equilibrated with 20 mM HEPES, 150 mM NaCl, pH 7.4. The resin was subsequently washed with 3 resin volumes (RV) of the same buffer before MAb P3.2 (Thermo Fisher) was eluted using 3 RV of 0.2 M glycine, pH 2.5. The pH of the solution was immediately neutralized with 1 M Tris-HCl, pH 7.5, to a final concentration of 50 mM, and MAb P3.2 was desalted in $1\times$ PBS. Papain digestion was performed overnight at room temperature (RT) using the Pierce Mouse IgG1 Fab and F(ab')$_2$ kit (Pierce), and Fc was separated from Fab fragments using protein A resin. Fab P3.2-containing aliquots were stored at -80°C in $1\times$ PBS. Monoclonal antibody 10C8 was prepared in a similar way except that SJL strain mice were coimmunized with both full-length P113EE and P113-Y1-N653 proteins (18). Immunized mice were tested for P113-specific antibody titers by ELISAs essentially as described previously (35). Hybridoma supernatants were screened for binding to P113EE, P113-Y1-N653, and P113-Y1-K197 proteins by ELISA. Further, clones were counterscreened against the rat Cd4-His protein to remove any antibodies reacting against the tag. The 10C8 monoclonal antibody was purified on a protein A column using standard methods. The antibody was eluted at pH 3.0 and dialyzed against PBS. The dialyzed antibody was sterile filtered and isotyped as IgG1/kappa. Binding to P113EE and P113-Y1-N653 protein was verified by ELISA.

ELISA. Protein expression levels and monoclonal antibody binding were quantified by ELISA essentially as described previously (36). Briefly, biotinylated proteins were immobilized in individual wells of streptavidin-coated microtiter plates and the appropriate primary antibody was added. To quantify protein expression levels, the mouse anti-rat Cd4 monoclonal antibody (OX68) which recognizes the Cd4 expression tag was used, and to determine the location of antibody epitopes, the anti-P113 MAbs P3.2 and 10C8 were added. An anti-mouse-alkaline phosphatase conjugate was used as a secondary antibody (Sigma, United Kingdom).

AVEXIS. *Av*idity-based *ex*tracellular *i*nteraction *s*creening (AVEXIS) was performed essentially as described previously (24). Briefly, monomeric biotinylated bait proteins and highly avid pentameric β-lactamase-tagged prey protein were prepared and their expression levels were normalized using enzyme activity to approximately 5 μg ml^{-1} prior to their use in interaction screening (33). Biotinylated baits were immobilized in streptavidin-coated 96-well microtiter plates, washed with PBST (PBS-0.1% Tween 20), incubated with prey proteins, and washed three times with PBST. Captured preys were quantified by adding the colorimetric β-lactamase substrate nitrocefin and measuring the absorbance of the hydrolysis products at 485 nm. The negative control in each screen was the query prey protein probed against the Cd4d3+4 tag alone.

Surface plasmon resonance analysis. Surface plasmon resonance studies were performed using a Biacore 8K instrument (GE Healthcare) as described previously (23). Biotinylated bait proteins were captured on a streptavidin-coated sensor chip (GE Healthcare). Approximately 400 response units (RU) of the negative-control bait (biotinylated rat Cd4d3+4) was immobilized on the reference flow cell, and

approximate molar equivalents of the query protein were immobilized in other flow cells. Purified analyte proteins were separated by size exclusion chromatography on a Superdex 200 Increase 10/300 column (GE Healthcare) in HBS-EP (10 mM HEPES, 150 mM NaCl, 3 mM EDTA, 0.05% [vol/vol] P20 surfactant) just prior to use in SPR experiments to remove any protein aggregates that might influence kinetic measurements. Increasing concentrations of purified proteins were injected at 100 μl/min to determine kinetic parameters or at 30 μl/min for equilibrium measurements. Both kinetic and equilibrium binding data were analyzed in Biacore 8K evaluation software version 1.1 (GE Healthcare). Equilibrium binding measurements were taken once equilibrium had been reached using reference-subtracted sensorgrams. Both the kinetic and equilibrium binding were replicated using independent protein preparations of both ligand and analyte proteins. All experiments were performed at 37°C in HBS-EP.

Determination of the structure of P113 bound to monoclonal antibody 3.2. P113$_{1-197}$ was combined with Fab P3.2 in a 1:1.2 (wt/wt) ratio for 1 h at room temperature before the lysine methylation method as described previously (37). Residual methylation reagents were neutralized by addition of 1 M Tris-HCl, pH 7.5, to a final concentration of 50 mM Tris-HCl, and the protein complex was concentrated to 2 mg ml^{-1} using 30-kDa-cutoff concentrators (Millipore) before injection into an S75 16/600 column (GE Healthcare) previously equilibrated with 20 mM Tris-HCl, 150 mM NaCl, pH 7.4. Fractions containing the P113$_{1-197}$:Fab P3.2 complex were pooled and concentrated to 10 mg ml^{-1} as appropriate for crystal formation based on use of a precrystallization kit (Hampton Research). Crystallization trials in 96-well plates were set up at 4°C with the sitting-drop method using commercial screens (ProPlex, Midas, Morpheus, MembFac, and MembGold2) with 100 nl reservoir plus 100-nl protein drops. Diamond-shaped crystals appeared in 7 to 10 days in 0.1 M Mg acetate, 0.1 morpholineethanesulfonic acid (MES) (pH 5.8), 22% (wt/vol) PEG 4000 and were supplemented with 20% (wt/vol) 2-methyl-2,4-pentanediol (MPD) before being flash cooled in liquid N$_2$. Two data sets from a single crystal were collected at 100 K at beamline I03 of the Diamond Light Source. The crystal belonged to space group P4$_1$2$_1$2 with unit cell dimensions a = 97 Å, b = 97 Å, c = 178 Å, and $\alpha = \beta = \gamma = 90°$. The data sets were indexed and reduced to 1.95-Å resolution using autoPROC (38). The R_{free} set, comprising 5% of the reflections, was generated randomly in Unique. The structure was solved by molecular replacement using as searching models the light and heavy chain of Fab 9AD4 (PDB ID: 4U0R), after pruning the side chains using chainsaw (CCP4 package [39]) and manually deleting the variable regions in the PDB. The two searching models were used sequentially in PHASER as implemented in Phenix MR (40). The MR solution was further extended using BUSTER (41) using the missing atoms option leading with initial R_{factor} and R_{free} of 41 and 45%, respectively.

The majority of P113$_{1-197}$ (163/197 amino acids) was initially built as a polyalanine model in PHENIX Autobuild, followed by multiple runs of restrained refinement in PHENIX (resolution range 50.58 to 1.95 Å). Reiterated model building was performed in COOT (42), and structure validation was performed using MOLPROBITY (43) before deposition in the PDB (PDB accession code 6Z2L). Crystallography data and refinement statistics are reported in Table 1. All the crystallographic programs were used as part of the SBGrid package (44). Structure homology was analyzed using the DALI server (45), while protein-protein interface was analyzed using PISA (46). Protein topology was produced using PDBsum (47), and protein images were produced using the graphic software PYMOL (48).

Hydrogen-deuterium exchange mass spectrometry. HDX-MS was performed using a Waters HDX manager composed of a nano-Acquity ultrahigh-pressure liquid chromatograph (UPLC) coupled to a Synapt G2-Si (Waters) mass spectrometer. Samples were prepared by 11-fold dilutions from 7 μM apo P113 in deuterated or nondeuterated and P113-10C8 or P113-RH5 complex in deuterated 20 mM HEPES, 150 mM NaCl (pH 7.4) buffer. The pH of the sample was reduced to 2.3 by adding 50% (vol/vol) 150 mM HCl. The apo protein and complexes were digested in-line using a pepsin-immobilized column at 20°C. The peptides generated from pepsin digestion were trapped on a micro-peptide trap for 2 min at a flow rate of 200 μl min^{-1}, to allow the removal of salts, and were then separated using a C$_{18}$ column with a linear gradient of 5 to 65% acetonitrile in water, both supplemented with 0.1% formic acid, for 9 min at flow rate of 40 μl min^{-1}. The temperature at which liquid chromatography was performed was set at 0°C to reduce back-exchange. Peptide mapping of P113 was performed by using nondeuterated samples in triplicate, and only unique peptides present in all three data files were selected for deuterium uptake data analysis. Apo P113 protein digestion provided a list of 1,649 peptides. After applying selection filters, and after manual inspection, 59 peptides were selected for analysis. These peptides provided ~95% sequence coverage with many overlapping peptides. For labeling experiments, apo P113, P113-10C8, or P113-RH5 was incubated for 20 s, 10 min, and 2 h in deuterated buffer. All HDX-MS experiments were performed in duplicate. Sequence coverage and deuterium uptake were analyzed by using ProteinLynx Global Server (Waters) and DynamX (Waters) programs, respectively. Leucine enkephalin at a continuous flow rate of 5 μl min^{-1} was sprayed as a lock mass for mass correction.

***P. falciparum* culture and growth inhibition activity assays.** The ability of anti-P113 MAbs to inhibit *in vitro* growth of *P. falciparum* 3D7 parasites was assessed using a standardized procedure. The MAbs were buffer exchanged against incomplete culture medium (25 mM HEPES, 0.37 mM hypoxanthine, and 2 mM L-glutamine in RPMI [Sigma; R0883]), concentrated with centrifugal filter devices (Amicon, Fisher Scientific; UFC901096), and sterilized by filtration through a 0.22-μm spin filter (Costar Spin-X; SLS Ltd.; catalog no. 8160) before use in the assay. These samples were tested in a serial 3-fold dilution with a start concentration of 1 mg ml^{-1} IgG in triplicate in a one-cycle growth inhibition activity (GIA) assay using human O$^+$ erythrocytes parasitized with mid-trophozoite stages of *P. falciparum* prepared by 5% sorbitol treatment on the previous day. Parasite growth after approximately 44 h of culture was determined by a biochemical assay specific for parasite lactate dehydrogenase (49). Values obtained with test IgGs were compared with those obtained with parasites incubated in the presence of

TABLE 1 Crystallographic statistics

Statistic	P113-Fab 3.2
Beamline	Diamond I03
Wavelength (Å)	0.9762
Resolution range (Å)	96.92—1.95 (2.00—1.95)
Space group	$P\,4_1\,2_1\,2$
Unit cell parameters	a = 96.92 Å, b = 96.92 Å, c = 177.90 Å, $\alpha = \beta = \gamma = 90.00°$
Total reflections, no.	1,636,680 (112,906)
Unique reflections, no.	62,581 (4,310)
Multiplicity	26.2 (26.2)
Completeness (%)	100.00 (100.00)
Mean I/sigma (I)	16.6 (1.70)
Wilson B-factor (Å^2)	41.80
R-merge	0.151 (5.073)
R-pim	0.042 (1.422)
$CC_{1/2}$	0.994 (0.571)
Reflections used in refinement, no.	62,481
Reflections used for R-free, no.	3,110
R_{work}	0.204
R_{free}	0.225
CC (work)	0.944
CC (free)	0.945
No. of nonhydrogen atoms	5,329
Macromolecules	4,929
Ligands	5
Solvent	395
Protein residues, no.	631
Root mean square derivation, bond lengths (Å)	0.012
Root mean square deviation, bond angles (°)	1.35
Ramachandran favored (%)	97.56
Ramachandran allowed (%)	2.44
Ramachandran outliers (%)	
Rotamer outliers (%)	0.71
Clashscore	3.5
Avg B-factor (Å^2)	43.14
Macromolecules	42.53
Ligands	79.98
Solvent	50.3
PDB ID	6Z2L

positive and negative controls (normal growth medium, 5 mM EDTA, and positive [RH5-specific] and negative-control MAbs).

Data availability. The coordinates and structure factors associated with this work are available at the Protein Data Bank (PDB: 6Z2L). All other data are available from the authors on request.

and antibody binding assays. S.M. and K.E.W. performed the HDX analysis under the supervision of A.P.S. L.K.B. cloned the P3.2 antibody, D.Q. performed the GIA assays, and both were supervised by S.J.D. T.W.P. and V.K. provided the 10C8 MAb and information regarding its development and characterization. M.K.H. and G.J.W. managed the project and analyzed data. I.C., F.G., M.K.H., and G.J.W. wrote the manuscript.

I.C., K.E.W., S.J.D., M.K.H., and G.J.W. are named inventors on patent applications relating to RH5-based malaria vaccines and/or antibodies.

REFERENCES

1. World Health Organization. 2019. World malaria report 2019. World Health Organization, Geneva, Switzerland.
2. Haldar K, Bhattacharjee S, Safeukui I. 2018. Drug resistance in Plasmodium. Nat Rev Microbiol 16:156–170. https://doi.org/10.1038/nrmicro.2017.161.
3. Cowman AF, Tonkin CJ, Tham W-H, Duraisingh MT. 2017. The molecular basis of erythrocyte invasion by malaria parasites. Cell Host Microbe 22:232–245. https://doi.org/10.1016/j.chom.2017.07.003.
4. Weiss GE, Gilson PR, Taechalertpaisarn T, Tham W-H, de Jong NWM, Harvey KL, Fowkes FJI, Barlow PN, Rayner JC, Wright GJ, Cowman AF, Crabb BS. 2015. Revealing the sequence and resulting cellular morphology of receptor-ligand interactions during Plasmodium falciparum invasion of erythrocytes. PLoS Pathog 11:e1004670. https://doi.org/10.1371/journal.ppat.1004670.
5. Crosnier C, Bustamante LY, Bartholdson SJ, Bei AK, Theron M, Uchikawa M, Mboup S, Ndir O, Kwiatkowski DP, Duraisingh MT, Rayner JC, Wright GJ. 2011. Basigin is a receptor essential for erythrocyte invasion by Plasmodium falciparum. Nature 480:534–537. https://doi.org/10.1038/nature10606.
6. Wright KE, Hjerrild KA, Bartlett J, Douglas AD, Jin J, Brown RE, Illingworth JJ, Ashfield R, Clemmensen SB, de Jongh WA, Draper SJ, Higgins MK. 2014. Structure of malaria invasion protein RH5 with erythrocyte basigin and blocking antibodies. Nature 515:427–430. https://doi.org/10.1038/nature13715.
7. Alanine DGW, Quinkert D, Kumarasingha R, Mehmood S, Donnellan FR, Minkah NK, Dadonaite B, Diouf A, Galaway F, Silk SE, Jamwal A, Marshall JM, Miura K, Foquet L, Elias SC, Labbé GM, Douglas AD, Jin J, Payne RO, Illingworth JJ, Pattinson DJ, Pulido D, Williams BG, de Jongh WA, Wright GJ, Kappe SHI, Robinson CV, Long CA, Crabb BS, Gilson PR, Higgins MK, Draper SJ. 2019. Human antibodies that slow erythrocyte invasion potentiate malaria-neutralizing antibodies. Cell 178:216–228.e21. https://doi.org/10.1016/j.cell.2019.05.025.
8. Bustamante LY, Bartholdson SJ, Crosnier C, Campos MG, Wanaguru M, Nguon C, Kwiatkowski DP, Wright GJ, Rayner JC. 2013. A full-length recombinant Plasmodium falciparum PfRH5 protein induces inhibitory antibodies that are effective across common PfRH5 genetic variants. Vaccine 31:373–379. https://doi.org/10.1016/j.vaccine.2012.10.106.
9. Douglas AD, Williams AR, Illingworth JJ, Kamuyu G, Biswas S, Goodman AL, Wyllie DH, Crosnier C, Miura K, Wright GJ, Long CA, Osier FH, Marsh K, Turner AV, Hill AVS, Draper SJ. 2011. The blood-stage malaria antigen PfRH5 is susceptible to vaccine-inducible cross-strain neutralizing antibody. Nat Commun 2:601. https://doi.org/10.1038/ncomms1615.
10. Douglas AD, Baldeviano GC, Lucas CM, Lugo-Roman LA, Crosnier C, Bartholdson SJ, Diouf A, Miura K, Lambert LE, Ventocilla JA, Leiva KP, Milne KH, Illingworth JJ, Spencer AJ, Hjerrild KA, Alanine DGW, Turner AV, Moorhead JT, Edgel KA, Wu Y, Long CA, Wright GJ, Lescano AG, Draper SJ. 2015. A PfRH5-based vaccine is efficacious against heterologous strain blood-stage Plasmodium falciparum infection in aotus monkeys. Cell Host Microbe 17:130–139. https://doi.org/10.1016/j.chom.2014.11.017.
11. Douglas AD, Baldeviano GC, Jin J, Miura K, Diouf A, Zenonos ZA, Ventocilla JA, Silk SE, Marshall JM, Alanine DGW, Wang C, Edwards NJ, Leiva KP, Gomez-Puerta LA, Lucas CM, Wright GJ, Long CA, Royal JM, Draper SJ. 2019. A defined mechanistic correlate of protection against Plasmodium falciparum malaria in non-human primates. Nat Commun 10:1953. https://doi.org/10.1038/s41467-019-09894-4.
12. Payne RO, Silk SE, Elias SC, Miura K, Diouf A, Galaway F, de Graaf H, Brendish NJ, Poulton ID, Griffiths OJ, Edwards NJ, Jin J, Labbé GM, Alanine DG, Siani L, Di Marco S, Roberts R, Green N, Berrie E, Ishizuka AS, Nielsen CM, Bardelli M, Partey FD, Ofori MF, Barfod L, Wambua J, Murungi LM, Osier FH, Biswas S, McCarthy JS, Minassian AM, Ashfield R,

Viebig NK, Nugent FL, Douglas AD, Vekemans J, Wright GJ, Faust SN, Hill AV, Long CA, Lawrie AM, Draper SJ. 2017. Human vaccination against RH5 induces neutralizing antimalarial antibodies that inhibit RH5 invasion complex interactions. JCI Insight 2:e96381. https://doi.org/10.1172/jci.insight.96381.
13. Dreyer AM, Matile H, Papastogiannidis P, Kamber J, Favuzza P, Voss TS, Wittlin S, Pluschke G. 2012. Passive immunoprotection of Plasmodium falciparum-infected mice designates the CyRPA as candidate malaria vaccine antigen. J Immunol 188:6225–6237. https://doi.org/10.4049/jimmunol.1103177.
14. Reddy KS, Amlabu E, Pandey AK, Mitra P, Chauhan VS, Gaur D. 2015. Multiprotein complex between the GPI-anchored CyRPA with PfRH5 and PfRipr is crucial for Plasmodium falciparum erythrocyte invasion. Proc Natl Acad Sci U S A 112:1179–1184. https://doi.org/10.1073/pnas.1415466112.
15. Volz JC, Yap A, Sisquella X, Thompson JK, Lim NTY, Whitehead LW, Chen L, Lampe M, Tham W-H, Wilson D, Nebl T, Marapana D, Triglia T, Wong W, Rogers KL, Cowman AF. 2016. Essential role of the PfRh5/PfRipr/CyRPA complex during Plasmodium falciparum invasion of erythrocytes. Cell Host Microbe 20:60–71. https://doi.org/10.1016/j.chom.2016.06.004.
16. Chen L, Lopaticki S, Riglar DT, Dekiwadia C, Uboldi AD, Tham W-H, O'Neill MT, Richard D, Baum J, Ralph SA, Cowman AF. 2011. An EGF-like protein forms a complex with PfRH5 and is required for invasion of human erythrocytes by Plasmodium falciparum. PLoS Pathog 7:e1002199. https://doi.org/10.1371/journal.ppat.1002199.
17. Baum J, Chen L, Healer J, Lopaticki S, Boyle M, Triglia T, Ehlgen F, Ralph SA, Beeson JG, Cowman AF. 2009. Reticulocyte-binding protein homologue 5—an essential adhesin involved in invasion of human erythrocytes by Plasmodium falciparum. Int J Parasitol 39:371–380. https://doi.org/10.1016/j.ijpara.2008.10.006.
18. Galaway F, Drought LG, Fala M, Cross N, Kemp AC, Rayner JC, Wright GJ. 2017. P113 is a merozoite surface protein that binds the N terminus of Plasmodium falciparum RH5. Nat Commun 8:14333. https://doi.org/10.1038/ncomms14333.
19. Wong W, Huang R, Menant S, Hong C, Sandow JJ, Birkinshaw RW, Healer J, Hodder AN, Kanjee U, Tonkin CJ, Heckmann D, Soroka V, Søgaard TMM, Jørgensen T, Duraisingh MT, Czabotar PE, de Jongh WA, Tham W-H, Webb AI, Yu Z, Cowman AF. 2019. Structure of Plasmodium falciparum Rh5-CyRPA-Ripr invasion complex. Nature 565:118–121. https://doi.org/10.1038/s41586-018-0779-6.
20. Sanders PR, Cantin GT, Greenbaum DC, Gilson PR, Nebl T, Moritz RL, Yates JR, III, Hodder AN, Crabb BS. 2007. Identification of protein complexes in detergent-resistant membranes of Plasmodium falciparum schizonts. Mol Biochem Parasitol 154:148–157. https://doi.org/10.1016/j.molbiopara.2007.04.013.
21. Elsworth B, Sanders PR, Nebl T, Batinovic S, Kalanon M, Nie CQ, Charnaud SC, Bullen HE, de Koning Ward TF, Tilley L, Crabb BS, Gilson PR. 2016. Proteomic analysis reveals novel proteins associated with the Plasmodium protein exporter PTEX and a loss of complex stability upon truncation of the core PTEX component, PTEX150. Cell Microbiol 18:1551–1569. https://doi.org/10.1111/cmi.12596.
22. Illingworth JJ, Alanine DG, Brown R, Marshall JM, Bartlett HE, Silk SE, Labbe GM, Quinkert D, Cho JS, Wendler JP, Pattinson DJ, Barfod L, Douglas AD, Shea MW, Wright KE, de Cassan SC, Higgins MK, Draper SJ. 2019. Functional comparison of blood-stage Plasmodium falciparum malaria vaccine candidate antigens. Front Immunol 10:1254. https://doi.org/10.3389/fimmu.2019.01254.
23. Galaway F, Yu R, Constantinou A, Prugnolle F, Wright GJ. 2019. Resurrection of the ancestral RH5 invasion ligand provides a molecular explanation for the origin of P falciparum malaria in humans. PLoS Biol 17:e3000490. https://doi.org/10.1371/journal.pbio.3000490.
24. Bushell KM, Söllner C, Schuster-Boeckler B, Bateman A, Wright GJ. 2008.

Large-scale screening for novel low-affinity extracellular protein interactions. Genome Res 18:622–630. https://doi.org/10.1101/gr.7187808.

25. Shirai T, Watanabe Y, Lee M-S, Ogawa T, Muramoto K. 2009. Structure of rhamnose-binding lectin CSL3: unique pseudo-tetrameric architecture of a pattern recognition protein. J Mol Biol 391:390–403. https://doi.org/10.1016/j.jmb.2009.06.027.

26. Vakonakis I, Langenhan T, Prömel S, Russ A, Campbell ID. 2008. Solution structure and sugar-binding mechanism of mouse latrophilin-1 RBL: a 7TM receptor-attached lectin-like domain. Structure 16:944–953. https://doi.org/10.1016/j.str.2008.02.020.

27. Jackson VA, del Toro D, Carrasquero M, Roversi P, Harlos K, Klein R, Seiradake E. 2015. Structural basis of latrophilin-FLRT interaction. Structure 23:774–781. https://doi.org/10.1016/j.str.2015.01.013.

28. Gilson PR, Nebl T, Vukcevic D, Moritz RL, Sargeant T, Speed TP, Schofield L, Crabb BS. 2006. Identification and stoichiometry of glycosylphosphatidylinositol-anchored membrane proteins of the human malaria parasite Plasmodium falciparum. Mol Cell Proteomics 5:1286–1299. https://doi.org/10.1074/mcp.M600035-MCP200.

29. Sanders PR, Gilson PR, Cantin GT, Greenbaum DC, Nebl T, Carucci DJ, McConville MJ, Schofield L, Hodder AN, Yates JR, III, Crabb BS. 2005. Distinct protein classes including novel merozoite surface antigens in Raft-like membranes of Plasmodium falciparum. J Biol Chem 280:40169–40176. https://doi.org/10.1074/jbc.M509631200.

30. Ragotte RJ, Higgins MK, Draper SJ. 2020. The RH5-CyRPA-Ripr complex as a malaria vaccine target. Trends Parasitol 36:545–559. https://doi.org/10.1016/j.pt.2020.04.003.

31. Wright GJ, Rayner JC. 2014. Plasmodium falciparum erythrocyte invasion: combining function with immune evasion. PLoS Pathog 10:e1003943. https://doi.org/10.1371/journal.ppat.1003943.

32. Crosnier C, Wanaguru M, McDade B, Osier FH, Marsh K, Rayner JC, Wright GJ. 2013. A library of functional recombinant cell-surface and secreted P falciparum merozoite proteins. Mol Cell Proteomics 12:3976–3986. https://doi.org/10.1074/mcp.O113.028357.

33. Kerr JS, Wright GJ. 2012. Avidity-based extracellular interaction screening (AVEXIS) for the scalable detection of low-affinity extracellular receptor-ligand interactions. J Vis Exp (61):e3881. https://doi.org/10.3791/3881.

34. Bartholdson SJ, Bustamante LY, Crosnier C, Johnson S, Lea S, Rayner JC, Wright GJ. 2012. Semaphorin-7A is an erythrocyte receptor for P falciparum merozoite-specific TRAP homolog, MTRAP. PLoS Pathog 8:e1003031. https://doi.org/10.1371/journal.ppat.1003031.

35. Staudt N, Müller-Sienerth N, Fane-Dremucheva A, Yusaf SP, Millrine D, Wright GJ. 2015. A panel of recombinant monoclonal antibodies against zebrafish neural receptors and secreted proteins suitable for wholemount immunostaining. Biochem Biophys Res Commun 456:527–533. https://doi.org/10.1016/j.bbrc.2014.11.123.

36. Elton CM, Rodriguez M, Ben Mamoun C, Lobo CA, Wright GJ. 2019. A library of recombinant Babesia microti cell surface and secreted proteins for diagnostics discovery and reverse vaccinology. Int J Parasitol 49:115–125. https://doi.org/10.1016/j.ijpara.2018.10.003.

37. Walter TS, Meier C, Assenberg R, Au K-F, Ren J, Verma A, Nettleship JE,

Owens RJ, Stuart DI, Grimes JM. 2006. Lysine methylation as a routine rescue strategy for protein crystallization. Structure 14:1617–1622. https://doi.org/10.1016/j.str.2006.09.005.

38. Vonrhein C, Flensburg C, Keller P, Sharff A, Smart O, Paciorek W, Womack T, Bricogne G. 2011. Data processing and analysis with the autoPROC toolbox. Acta Crystallogr D Biol Crystallogr 67:293–302. https://doi.org/10.1107/S0907444911007773.

39. Winn MD, Ballard CC, Cowtan KD, Dodson EJ, Emsley P, Evans PR, Keegan RM, Krissinel EB, Leslie AGW, McCoy A, McNicholas SJ, Murshudov GN, Pannu NS, Potterton EA, Powell HR, Read RJ, Vagin A, Wilson KS. 2011. Overview of the CCP4 suite and current developments. Acta Crystallogr D Biol Crystallogr 67:235–242. https://doi.org/10.1107/S0907444910045749.

40. Liebschner D, Afonine PV, Baker ML, Bunkóczi G, Chen VB, Croll TI, Hintze B, Hung LW, Jain S, McCoy AJ, Moriarty NW, Oeffner RD, Poon BK, Prisant MG, Read RJ, Richardson JS, Richardson DC, Sammito MD, Sobolev OV, Stockwell DH, Terwilliger TC, Urzhumtsev AG, Videau LL, Williams CJ, Adams PD. 2019. Macromolecular structure determination using X-rays, neutrons and electrons: recent developments in Phenix. Acta Crystallogr D Struct Biol 75:861–877. https://doi.org/10.1107/S2059798319011471.

41. Blanc E, Roversi P, Vonrhein C, Flensburg C, Lea SM, Bricogne G. 2004. Refinement of severely incomplete structures with maximum likelihood in BUSTER-TNT. Acta Crystallogr D Biol Crystallogr 60:2210–2221. https://doi.org/10.1107/S0907444904016427.

42. Emsley P, Lohkamp B, Scott WG, Cowtan K. 2010. Features and development of Coot. Acta Crystallogr D Biol Crystallogr 66:486–501. https://doi.org/10.1107/S0907444910007493.

43. Chen VB, Arendall WB, III, Headd JJ, Keedy DA, Immormino RM, Kapral GJ, Murray LW, Richardson JS, Richardson DC. 2010. MolProbity: all-atom structure validation for macromolecular crystallography. Acta Crystallogr D Biol Crystallogr 66:12–21. https://doi.org/10.1107/S0907444909042073.

44. Morin A, Eisenbraun B, Key J, Sanschagrin PC, Timony MA, Ottaviano M, Sliz P. 2013. Collaboration gets the most out of software. Elife 2:e01456. https://doi.org/10.7554/eLife.01456.

45. Holm L, Rosenström P. 2010. Dali server: conservation mapping in 3D. Nucleic Acids Res 38:W545–W549. https://doi.org/10.1093/nar/gkq366.

46. Krissinel E, Henrick K. 2007. Inference of macromolecular assemblies from crystalline state. J Mol Biol 372:774–797. https://doi.org/10.1016/j.jmb.2007.05.022.

47. Laskowski RA, Jabłońska J, Pravda L, Vařeková RS, Thornton JM. 2018. PDBsum: structural summaries of PDB entries. Protein Sci 27:129–134. https://doi.org/10.1002/pro.3289.

48. DeLano WL. 2002. PyMOL: an open-source molecular graphics tool. CCP4 Newsl Protein Crystallogr (40):82–92.

49. Malkin EM, Diemert DJ, McArthur JH, Perreault JR, Miles AP, Giersing BK, Mullen GE, Orcutt A, Muratova O, Awkal M, Zhou H, Wang J, Stowers A, Long CA, Mahanty S, Miller LH, Saul A, Durbin AP. 2005. Phase 1 clinical trial of apical membrane antigen 1: an asexual blood-stage vaccine for Plasmodium falciparum malaria. Infect Immun 73:3677–3685. https://doi.org/10.1128/IAI.73.6.3677-3685.2005.